NMRCloudQ: A Quantum Cloud Experience on a Nuclear Magnetic Resonance Quantum Computer

Tao Xin,[1] Shilin Huang,[2] Sirui Lu,[1] Keren Li,[1] Zhihuang Luo,[3, 4] Zhangqi
Yin,[2] Jun Li,[3, 4, *] Dawei Lu,[5, 4, †] Guilu Long,[1, ‡] and Bei Zeng[6, 4]

[1]*Department of Physics, Tsinghua University, Beijing 100084, China*
[2]*Center for Quantum Information, Institute for Interdisciplinary*
Information Sciences, Tsinghua University, Beijing 100084, China
[3]*Beijing Computational Science Research Center, Beijing 100193, China*
[4]*Institute for Quantum Computing, University of Waterloo, Waterloo N2L 3G1, Ontario, Canada*
[5]*Department of Physics, Southern University of Science and Technology, Shenzhen 518055, China*
[6]*Department of Mathematics & Statistics, University of Guelph, Guelph N1G 2W1, Ontario, Canada*

As of today, no one can tell when a universal quantum computer with thousands of logical quantum bits (qubits) will be built. At present, most quantum computer prototypes involve less than ten individually controllable qubits, and only exist in laboratories for the sake of either the great costs of devices or professional maintenance requirements. Moreover, scientists believe that quantum computers will never replace our daily, every-minute use of classical computers, but would rather serve as a substantial addition to the classical ones when tackling some particular problems. Due to the above two reasons, cloud-based quantum computing is anticipated to be the most useful and reachable form for public users to experience with the power of quantum. As initial attempts, IBM Q has launched influential cloud services on a superconducting quantum processor in 2016, but no other platforms has followed up yet. Here, we report our new cloud quantum computing service – NMRCloudQ (http://nmrcloudq.com/zh-hans/), where nuclear magnetic resonance, one of the pioneer platforms with mature techniques in experimental quantum computing, plays as the role of implementing computing tasks. Our service provides a comprehensive software environment preconfigured with a list of quantum information processing packages, and aims to be freely accessible to either amateurs that look forward to keeping pace with this quantum era or professionals that are interested in carrying out real quantum computing experiments in person. In our current version, four qubits are already usable with in average 1.26% single-qubit gate error rate and 1.77% two-qubit controlled-NOT gate error rate via randomized benchmaking tests. Improved control precisions as well as a new seven-qubit processor are also in preparation and will be available later.

Building universal quantum computers requires highly developed control technology on physical systems at the quantum level. In recent years, quantum engineering technology, including preparation, manipulation, and detection of quantum systems, is undergoing rapid progress. Quantum computing devices built on a variety of underlying physical implementations are reaching unprecedented level of control and precision in laboratories around the world. Along with this trend, researchers are also making small-sized quantum simulators or processors available to the public by delivering them on the cloud [1, 2]. The primary benefit of cloud-based quantum computation is to enable independent parties to validate their ideas or to benchmark quantum operations of interest.

In this new rising field of cloud quantum computing, the superconducting group in IBM has made first steps in 2016 [1]. IBM provided the first commercial quantum computing service via a web based interface called IBM Quantum Experience. The underlying quantum hardware is a universal 5-qubit quantum computer based on superconducting transmon qubits. During its one-year service, IBM has provided a unique user experience and shed light on how to successfully maintain a server. In addition, vast amounts of data are obtained, while many of them are scientifically valuable [3, 4].

In this work, we provide online availability of another actual quantum hardware, which is based on a nuclear magnetic resonance (NMR) spectrometer. NMR spectroscopy is arguably one of the most versatile analytic methods for investigating quantum computation and quantum control [5]. However, an NMR quantum processor (spectrometer), due to its great cost and professional maintenance requirement, is not easy for the public to gain operating experiences. In order to allow for more people, either amateurs or professionals, to embrace and more importantly participate in the tidal wave of quantum science, we launched our NMR quantum cloud computing (NMRCloudQ) service. Through NMRCloudQ, we offer direct access to a real, physical spectrometer in our lab and encourage users to explore quantum phenomena and demonstrate quantum algorithms.

In this paper, we first review some of the most important progresses in NMR quantum computing during the past two decades, and then briefly explain the basics of NMR quantum computing and how to access our cloud service. Finally, we discuss the results and propose po-

---
* junli@csrc.ac.cn
† ludw@sustc.edu.cn
‡ gllong@tsinghua.edu.cn

tential improvements of NMRCloudQ.

I. NMR QUANTUM COMPUTING

Since the emergence of Shor's factoring algorithm [6] lit the world's fervor in pursuing quantum computers more than two decades ago, nuclear magnetic resonance (NMR) has always been one of the pioneer platforms to tackle a variety of quantum information tasks, ranging from the development of advanced control techniques [5] to implementation of quantum algorithms [7]. Very soon after the ideas on how to build NMR quantum computers [8, 9], initial attempts towards the implementation of Grover's search algorithm [10] and Shor's factoring algorithm [11], and coherent control of up to 7 qubits [12] have been successively realized. Such rapid progress in NMR quantum computing during the early years can be majorly attributed to the mature skills in pulse design and optimization, which are accumulated along the history of NMR spectroscopy.

On the other hand, the new application in quantum computing also brings traditional NMR community new technologies, where we would mention the gradient ascent pulse engineering (GRAPE) algorithm [13] as a typical example. GRAPE techniques were firstly proposed to achieve high-fidelity controls of individual spins, as well as the entire system dynamics, to satisfy the rigid requirements of a quantum computer. At present, it has been an important pulse engineering approach in NMR spectroscopy, and is also widely used in other quantum computing architectures including election spin resonance [14], nitrogen-vacancy centers in diamond [15, 16], superconducting circuits [17, 18], and ion traps [19, 20]. In particular, the control fidelities for single-qubit gates 99.97% and two-qubit gates 99.5% [21] demonstrated via randomized benchmarking in NMR still remain as one of the best in experimental quantum computing to date.

After two decades of the initial idea about NMR quantum computing, we launched the first cloud quantum computing service based on NMR, i.e. NMRCloudQ.

II. CONFIGURATION OF NMRCLOUDQ

A rich variety of software applications for processing and analyzing NMR experimental spectra has been involved, enabling the automation of many complex tasks in quantum information processing. With the feature-rich and sophisticated software functionality developed in the magnetic resonance community, we can reasonably conclude that most liquid-state NMR quantum computing experiments can now be automated with relative ease.

The connections between different parts can be illustrated as shown in Fig. 1

Our quantum processor is functionalized on a molecule ^{13}C-labeled trans-crotonic acid $(C_4H_6O_2)$ dissolved in d6-acetone. This sample contains four carbons and five
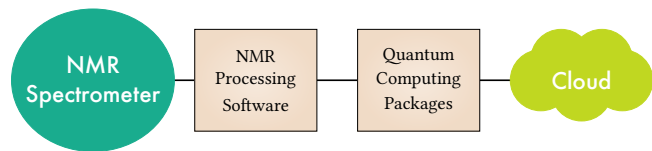

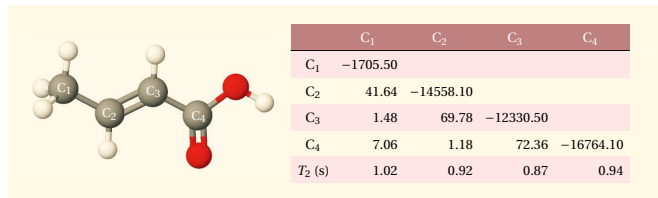FIG. 1. Connection between different parts of our automated system.

	C_1	C_2	C_3	C_4
C_1	−1705.50			
C_2	41.64	−14558.10		
C_3	1.48	69.78	−12330.50	
C_4	7.06	1.18	72.36	−16764.10
T_2 (s)	1.02	0.92	0.87	0.94

FIG. 2. Molecular structure and Hamiltonian parameters of ^{13}C-labeled trans-crotonic acid. In experiments, C_1, C_2, C_3 and C_4 are used as a 4-qubit quantum processor. In the table, the chemical shifts and J-couplings (in Hz) are given as the diagonal and off-diagonal elements, respectively. The last row of the table shows the values of T_2.

protons, where the protons can be decoupled throughout experiments. Hence, we get a 4-qubit system, in which we label C_1 to C_4 as qubits 1 to 4. See Fig. 2 for the molecular structure and its Hamiltonian parameters. Experiments are carried out on a Bruker AVANCE 400 MHz spectrometer in our lab at room temperature.

The Hamiltonian of the system under weak coupling approximation is written as

$$H_S = \sum_{j=1}^{4} \pi \nu_j \sigma_z^j + \sum_{j<k,=1}^{4} \frac{\pi}{2} J_{jk} \sigma_z^j \sigma_z^k, \tag{1}$$

where ν_j is the Larmor frequency of the jth spin and J_{jk} is the J-coupling strength between the jth and the kth spin.

The manufacturer Bruker provides a software `TopSpin` to control the spectrometer. NMR experiments are routinely done with typing commands through `TopSpin`. This workstation enables users to build their own customized experiment libraries and set up sophisticated experiments, with multiple options provided. Combining `TopSpin` with our NMR quantum computing packages, it is able to access various types of quantum information experiments remotely.

III. NMR QUANTUM COMPUTING PACKAGES

Generally, a quantum computing experiment contains the following steps:

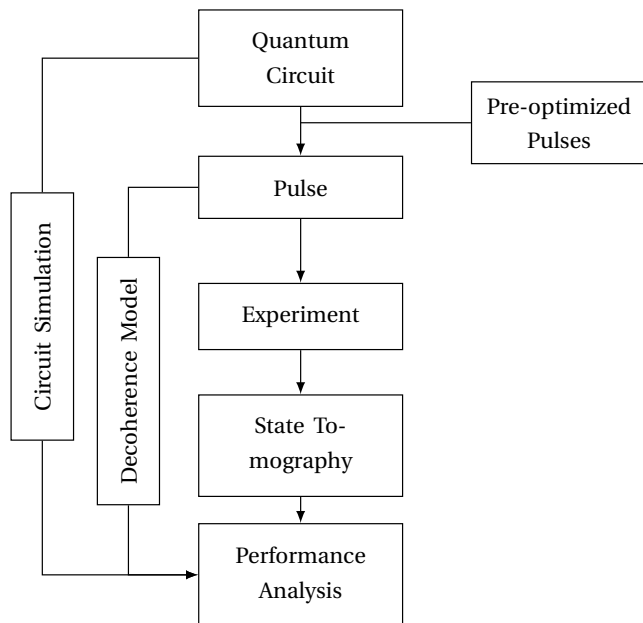(1) initial state preparation;
(2) implementing a quantum circuit;

tion of the maximally mixed state and a pure state

$$\rho_{pps} = (1 - \eta)\frac{I^{\otimes 4}}{2^4} + \eta|0^{\otimes 4}\rangle\langle 0^{\otimes 4}|, \qquad (4)$$

where η is a parameter characterizing the effective purity of the PPS, and its value is in the magnitude of ϵ. Although PPS is highly mixed, the operator $I^{\otimes 4}$ does not evolve under any unitary propagator nor is it observed in NMR spectra. Hence, only the deviated part $|0^{\otimes 4}\rangle\langle 0^{\otimes 4}|$ contributes to experimentally observable signal. It appears that PPS is just as suitable as the real pure state for quantum computing experiments.

We used the spatial averaging method [25] to make the transformation $\rho_{eq} \to \rho_{pps}$. Full state tomography is then performed in order to obtain a quantitative estimation of the quality of our PPS. We found that the fidelity between the prepared PPS and the target state is 98.77%. This state serves as the starting point for subsequent computation tasks.

B. Pulse Control for Executing Quantum Circuits

Any quantum circuit can be decomposed into a sequence of elementary quantum gates. It would be ideal to provide the availability of a set of universal set of gates, such as the Clifford gates plus T gate. However, due to the structure of our molecule, non nearest-neighboring CNOT gates are difficult to generate since the couplings are too small. So we do not provide CNOT gates between arbitrary two qubits but only nearest-neighbor ones. All pre-computed pulses are listed in Table I, while they still form a universal set of gates.

Finding appropriate control pulses to implement the target quantum operation is crucial for quantum computing experiments. A variety of numerical pulse-searching methods have been developed. The employment of optimal control theory to solve this problem proves to be a great success. In small-size systems, currently the most popular method in NMR is the gradient ascent pulse engineering (GRAPE) [13]. Through the GRAPE optimal control technique, high-accuracy control pulses can be found promptly in a 4-qubit system. In Table I, the pulses were optimized to be around 99.9% fidelity, and were also designed to be robust over a range of r.f. powers ($\pm5\%$ from the ideal power). Although not time-optimal, these pulses have smooth shapes and relatively low powers to reduce the probe heating in a long sequence.

Knowing the errors of a single gate in simulation is not sufficient for assessing the errors present in an actual quantum computation. In practice, the device suffers from systematic errors which may even vary between calibrations. To get a quantitative characterization of the real evolution when we apply a pulse, we use randomized benchmarking (RB) protocols [26]. RB has been implemented in many experimental platforms [21, 27–30]. Performing RB on our device is an important task for assess-

FIG. 3. Schematic workflow of our four-qubit NMR quantum computing cloud.

(3) measurement.

On the 4-qubit NMR quantum cloud, see Fig. 3, we have stored a bunch of pre-optimized pulses. These pulses are used to implement elementary single-qubit and two-qubit quantum gates. Now let us describe the procedure of cloud computing step by step.

A. Initial State Preparation

To run a quantum algorithm, we usually need to initialize the system to a pure state, say $|0\rangle^{\otimes n}$. In NMR quantum computing, the low polarization of the system at room temperature prevents us from generating a genuine pure state. To see this, we write down the form of the system's equilibrium state ρ_{eq}, which follows Boltzmann distribution at room temperature T:

$$\rho_{eq} = \frac{e^{-\beta H_S}}{\mathrm{Tr}\left(e^{-\beta H_S}\right)}, \qquad (2)$$

where $\beta = 1/(k_B T)$ (k_B is the Boltzmann constant). Since $\|H_S\|/(k_B T) \ll 1$,

$$\rho_{eq} \simeq \frac{I^{\otimes 4}}{2^4} - \beta H_S \simeq \frac{I^{\otimes 4}}{2^4} + \epsilon \sum_{j=1}^{4} \sigma_z^j, \qquad (3)$$

where Eq. (1) is substituted with coupling terms omitted, and ϵ is the polarization of the jth spin which is in the order of 10^{-5}.

To initialize the NMR system, the idea of pseudo-pure state (PPS) was introduced [22–24]. PPS is a combina-

Pulse name	Target gate	Pulse duration	No. of Slices	Numerical fidelity
NMRcloud_H_C1	Hadamard1	1ms	500	0.9989
NMRcloud_H_C2	Hadamard2	1ms	500	0.9992
NMRcloud_H_C3	Hadamard3	1ms	500	0.9943
NMRcloud_H_C4	Hadamard4	1ms	500	0.9943
NMRcloud_90_C1	$R_x^1(\pi/2)$	1ms	500	0.9989
NMRcloud_90_C2	$R_x^2(\pi/2)$	1ms	500	0.9986
NMRcloud_90_C3	$R_x^3(\pi/2)$	1ms	500	0.9993
NMRcloud_90_C4	$R_x^4(\pi/2)$	1ms	500	0.9991
NMRcloud_180_C1	$R_x^1(\pi)$	1ms	500	0.9992
NMRcloud_180_C2	$R_x^2(\pi)$	1ms	500	0.9991
NMRcloud_180_C3	$R_x^3(\pi)$	1ms	500	0.9994
NMRcloud_180_C4	$R_x^4(\pi)$	1ms	500	0.9991
NMRcloud_T_C1	T-gate1	1ms	500	0.9987
NMRcloud_T_C2	T-gate2	1ms	500	0.9992
NMRcloud_T_C3	T-gate3	1ms	500	0.9987
NMRcloud_T_C4	T-gate4	1ms	500	0.9990
NMRcloud_TD_C1	$T^\dagger$-gate1	1ms	500	0.9992
NMRcloud_TD_C2	$T^\dagger$-gate2	1ms	500	0.9991
NMRcloud_TD_C3	$T^\dagger$-gate3	1ms	500	0.9994
NMRcloud_TD_C4	$T^\dagger$-gate4	1ms	500	0.9991
NMRcloud_cnot_C12	$CNOT_{12}$	15ms	5000	0.9995
NMRcloud_cnot_C21	$CNOT_{21}$	15ms	5000	0.9999
NMRcloud_cnot_C23	$CNOT_{23}$	7.5ms	2500	0.9996
NMRcloud_cnot_C32	$CNOT_{32}$	7.5ms	2500	0.9999
NMRcloud_cnot_C34	$CNOT_{34}$	9ms	3000	0.9998
NMRcloud_cnot_C43	$CNOT_{43}$	9ms	3000	0.9999
NMRcloud_swap_C12	$SWAP_{12}$	40ms	4000	0.9995
NMRcloud_swap_C23	$SWAP_{23}$	40ms	4000	0.9998
NMRcloud_swap_C34	$SWAP_{34}$	30ms	3000	0.9996

TABLE I. GRAPE pulses for universal quantum gates, including 12 single-qubit gates, 6 CNOT gates and 3 SWAP gates.

ing its prospects with regards to achieving high-fidelity quantum control.

We have implemented RB to characterize the average single-qubit gate and two-qubit gate error rates. Their values are 1.26% and 1.77%, respectively. More details, such as the average error rate for each gate listed in Table. I, will come soon.

C. NMR State Tomography

NMR detection is performed on a bulk ensemble of molecules, hence the readout is an ensemble–averaged macroscopic measurement. All experimental data are extracted from the free-induction decay (FID), which is the signal induced by the precessing magnetization of the sample in a surrounding detection coil. FID is recorded as a time-domain signal, which consists of a number of oscillating waves of different frequencies, amplitudes, and phases. The signal is then subjected to Fourier transformation, and the resulting spectral lines are fitted, yielding a set of measurement data.

For our system, the direct observables are single-

coherent operators, i.e., only one qubit is in σ_x or σ_y while all the others are in σ_z or I. When measuring other operators, we apply additional readout pulses before data acquisition. For example, to measure a three-coherent operator $\sigma_x^1\sigma_y^2\sigma_y^3$, we need to rotate it to a single coherence $\sigma_x^1\sigma_z^2\sigma_z^3$ via a readout pulse $\exp(-i\pi/4\sigma_x^2) \otimes \exp(-i\pi/4\sigma_x^3)$. Therefore, to realize a full 4-qubit state reconstruction, we need a set of different readout pulses as listed in Table II, where all numerical fidelities are over 0.995.

D. Numerical Simulation

Computations are naturally subject to systematic errors. To estimate the imperfection of the optimized pulses, we provide three sets of data for user to evaluate the performance: (1) simulated results with the ideal quantum circuit; (2) simulated results with the optimized pulses, without and with consideration of decoherence; (3) experimentally measured results.

When user submits a quantum circuit, our server will immediately generate the corresponding pulse that im-

Pulse name	Target gate	Pulse duration
$IIII$	$identity$	0.9ms
$XXXX$	$R_x^{1234}(\pi/2)$	0.9ms
$IIYY$	$R_y^{34}(\pi/2)$	0.9ms
$YYXX$	$R_y^{12}(\pi/2)R_x^{34}(\pi/2)$	0.9ms
$IIIY$	$R_y^{4}(\pi/2)$	0.9ms
$XYXX$	$R_x^{134}(\pi/2)R_y^{2}(\pi/2)$	0.9ms
$YXYI$	$R_y^{13}(\pi/2)R_x^{2}(\pi/2)$	0.9ms
$IYXI$	$R_y^{2}(\pi/2)R_x^{3}(\pi/2)$	0.9ms
$IIIX$	$R_x^{4}(\pi/2)$	0.9ms
$XIYY$	$R_x^{1}(\pi/2)R_y^{34}(\pi/2)$	0.9ms
$YXII$	$R_y^{1}(\pi/2)R_x^{2}(\pi/2)$	0.9ms
$YYXY$	$R_y^{124}(\pi/2)R_x^{3}(\pi/2)$	0.9ms
$XYXI$	$R_x^{13}(\pi/2)R_y^{2}(\pi/2)$	0.9ms
$IIYX$	$R_y^{3}(\pi/2)R_x^{4}(\pi/2)$	0.9ms
$IXIY$	$R_x^{2}(\pi/2)R_y^{4}(\pi/2)$	0.9ms
$IIXI$	$R_x^{3}(\pi/2)$	0.9ms
$IYIY$	$R_y^{24}(\pi/2)$	0.9ms

TABLE II. Pulse set to implement 4-qubit state tomography on NMRCloudQ.

plements the circuit. A simulating program then computes the performance of the generated pulse. Suppose the pulse is of duration t and consists of M slices, then the time propagator will be

$$U(t) = \exp(-iH_M\tau)\cdots\exp(-iH_1\tau), \quad (5)$$

where H_m $(m = 1,...,M)$ represents the total Hamiltonian of the mth slice and $\tau = t/M$ is the duration of each slice.

For our NMR quantum computing hardware, errors majorly stem from decoherence. The relaxation mechanism is usually described by an independent decoherence model, that is, the qubits undergo uncorrelated channels, parameterized with the set of T_1^i and T_2^i $(i = 1, 2, 3, 4)$ per evolution time step τ. Our cloud provides a simulator to mimic what is happening under this error model. To be concrete, the density matrix $\hat{\rho}$ of the system is, at each evolution step, subjected to the composition of the error channels $\mathcal{E}_i$ for each qubit [31]

$$\rho \rightarrow \mathcal{E}_4 \circ \mathcal{E}_3 \circ \mathcal{E}_2 \circ \mathcal{E}_1(\rho), \quad (6)$$

where $\mathcal{E}_i$ represents the generalized amplitude damping and phase damping channel for the ith qubit. The simulated dynamics will also be shown online. Users are advised to use such data to characterize the discrepancies between theoretical and experimental results.

IV. OUTLOOK AND CONCLUSION

The primary bottleneck that limits our 4-qubit cloud computing service is the pulse control precision. In average, the single-qubit gate error rate is 1.26% and CNOT gate error rate is 1.77%, which are not state-of-the-art yet [21]. Actually, there are a few techniques to be applied in the near future, as follows.

For the single-qubit controls, the error mainly comes from the pulse optimization procedure and inhomogeneities of the magnetic field across the sample. We used 99.5% as the preset fidelity to optimize the pulse shape, which can be further set higher to 99.99%. In addition, the generated pulse will also be rectified using the feedback control technique to guarantee that the pulse performance on the spectrometer is the same as the generated one [32]. For the inhomogeneity problem, we intend to apply the r.f. selection technique [21], where only a portion of the NMR sample is chosen to run tasks by destroying the other's contribution to the final signal. This can be realized by a r.f. selection sequence. The selected portion of sample feels the most homogenous magnetic field, i.e., signal-to-noise (SNR) ratio will be greatly enhanced. The drawback is that the absolute signal decreases, since only that portion but not the entire sample makes contributions to it. This drawback may lead to more repetitions of experiments and hence more running time to gain a sufficiently strong signal.

For the two-qubit controls, the error mainly comes from decoherence. The length of a CNOT gate in general requires $\mathcal{O}\left(\frac{1}{2J}\right)$ time, where J is the coupling strength between two spins. In our 4-qubit processor, the largest J is about 70 Hz, leading to a 7 ms CNOT gate. The T_2^* time of each spin is around 400 ms, so a rough estimation of the decoherence error occurring in a CNOT gate should be more than 1%. The optimization based on the brachistochrone approach is a potential solution, but it will not improve much. Alternatively, we intend to use another sample iodotrifluroethylene (C_2F_3I), as the 4-qubit processor. Its couplings are around 200 Hz (roughly 2.5 ms CNOT gates), in comparison with the T_2^* time 600 ms, which in principle promises much more accurate CNOT gates.

The molecule of crotonic acid can also serve as a 7-qubit quantum processor. Besides the four ^{13}C spins, the molecule has five ^{1}H spins, while three of them form a methyl group. The methyl group, usually treated as a combination of a spin-3/2 particle and a spin-1/2 particle, can be indeed used as one qubit after the spin-1/2 part is selected [12]. Therefore, the crotonic acid can at most provide 7 qubits, and its cloud service is already in preparation.

In conclusion, cloud-based computation is an effective method for the storage and distribution of NMR data to the quantum computing community. It is our goal, in this project, to bring the state-of-the-art NMR quantum processor on-line. Our approach allows users to submit their quantum computing tasks to an automation queue and access their data remotely, i.e., without operating the NMR spectrometer in person. At current stage, it would be of great interest for users to run certain benchmarking circuits on the platform and demonstrate its performance. Ongoing efforts will be devoted to developing an automated computing setup with higher control pre-

cisions and more qubits. We expect that this work can make contributions to the enhancement of understandings in NMR quantum control and quantum computing to the wide public.

[1] IBM, The quantum experience, 2016, http://research.ibm.com/ibm-q/.
[2] Center for quantum photonics, quantum in the cloud, 2016, https://cnotmz.appspot.com/doc.
[3] K. Michielsen, M. Nocon, D. Willsch, F. Jin, T. Lippert, and H. D. Raedt, Comput. Phys. Commun. **220**, 44 (2017).
[4] S. J. Devitt, Phys. Rev. A **94**, 032329 (2016).
[5] L. M. Vandersypen and I. L. Chuang, Rev. Mod. Phys. **76**, 1037 (2005).
[6] P. W. Shor, in *Foundations of Computer Science, 1994 Proceedings., 35th Annual Symposium on* (Ieee, 1994) pp. 124–134.
[7] J. Jones, Prog. Nucl. Magn. Reson. Spectrosc. **59**, 91 (2011).
[8] D. G. Cory, A. F. Fahmy, and T. F. Havel, Proceedings of the National Academy of Sciences **94**, 1634 (1997).
[9] N. A. Gershenfeld and I. L. Chuang, Science **275**, 350 (1997).
[10] J. Jones, M. Mosca, and R. Hansen, NATURE **393**, 344 (1998).
[11] L. M. Vandersypen, M. Steffen, G. Breyta, C. S. Yannoni, M. H. Sherwood, and I. L. Chuang, Nature **414**, 883 (2001).
[12] E. Knill, R. Laflamme, R. Martinez, and C. Tseng, Nature **404**, 368 (2000).
[13] N. Khaneja, T. Reiss, C. Kehlet, T. Schulte-Herbrüggen, and S. J. Glaser, J. Magn. Reson. **172**, 296 (2005).
[14] Y. Zhang, C. A. Ryan, R. Laflamme, and J. Baugh, Phys. Rev. Lett. **107**, 170503 (2011).
[15] G. Waldherr, Y. Wang, S. Zaiser, M. Jamali, T. Schulte-Herbrüggen, H. Abe, T. Ohshima, J. Isoya, J. Du, P. Neumann, *et al.*, Nature **506**, 204 (2014).
[16] F. Dolde, V. Bergholm, Y. Wang, I. Jakobi, B. Naydenov, S. Pezzagna, J. Meijer, F. Jelezko, P. Neumann, T. Schulte-Herbrüggen, *et al.*, Nat. Commun. **5** (2014).
[17] F. Motzoi, J. Gambetta, P. Rebentrost, and F. K. Wilhelm, Phys. Rev. Lett. **103**, 110501 (2009).
[18] D. J. Egger and F. K. Wilhelm, Supercond. Sci. Technol. **27**, 014001 (2013).
[19] V. Nebendahl, H. Häffner, and C. Roos, Phys. Rev. A **79**, 012312 (2009).
[20] P. Schindler, J. T. Barreiro, T. Monz, V. Nebendahl, D. Nigg, M. Chwalla, M. Hennrich, and R. Blatt, Science **332**, 1059 (2011).
[21] C. Ryan, M. Laforest, and R. Laflamme, New J. Phys. **11**, 013034 (2009).
[22] N. A. Gershenfeld and I. L. Chuang, Science **275**, 350 (1997).
[23] D. G. Cory, M. D. Price, and T. F. Havel, Physica D **120**, 82 (1998).
[24] E. Knill, I. Chuang, and R. Laflamme, Phys. Rev. A **57**, 3348 (1998).
[25] M. Pravia, E. Fortunato, Y. Weinstein, M. D. Price, G. Teklemariam, R. J. Nelson, Y. Sharf, S. Somaroo, C. H. Tseng, T. F. Havel, and D. G. Cory, Concept. Magn. Reson. **11**, 225 (1999).
[26] J. Emerson, R. Alicki, and K. Zyczkowski, J. Opt. B **7**, S347 (2005).
[27] E. Knill, D. Leibfried, R. Reichle, J. Britton, R. B. Blakestad, J. D. Jost, C. Langer, R. Ozeri, S. Seidelin, and D. J. Wineland, Phys. Rev. A **77**, 012307 (2008).
[28] J. M. Chow, J. M. Gambetta, L. Tornberg, J. Koch, L. S. Bishop, A. A. Houck, B. R. Johnson, L. Frunzio, S. M. Girvin, and R. J. Schoelkopf, Phys. Rev. Lett. **102**, 090502 (2009).
[29] H. Paik, D. I. Schuster, L. S. Bishop, G. Kirchmair, G. Catelani, A. P. Sears, B. R. Johnson, M. J. Reagor, L. Frunzio, L. I. Glazman, S. M. Girvin, M. H. Devoret, and R. J. Schoelkopf, Phys. Rev. Lett. **107**, 240501 (2011).
[30] X. Rong, J. Geng, F. Shi, Y. Liu, K. Xu, W. Ma, F. Kong, Z. Jiang, Y. Wu, and J. Du, Nat. Commun. **6** (2015).
[31] M. A. Nielsen and I. L. Chuang, *Quantum Computation and Quantum Information* (Cambridge University Press, 2010).
[32] D. Lu, H. Li, D.-A. Trottier, J. Li, A. Brodutch, A. P. Krismanich, A. Ghavami, G. I. Dmitrienko, G. Long, J. Baugh, *et al.*, Phys. Rev. Lett. **114**, 140505 (2015).